The Astronomical Journal, 163:104 (10pp), 2022 March https://doi.org/10.3847/1538-3881/ac46c9

The Breakthrough Listen Search for Intelligent Life: Technosignature Search of Transiting TESS Targets of Interest

Noah Franz[1,2], Steve Croft[1,3], Andrew P. V. Siemion[1,3,4], Raffy Traas[1,5], Bryan Brzycki[1], Vishal Gajjar[1], Howard Isaacson[1,6], Matthew Lebofsky[1], David H. E. MacMahon[1], Danny C. Price[1,7], Sofia Z. Sheikh[1,3], Julia DeMarines[1], Jamie Drew[8], and S. Pete Worden[8]

[1] Department of Astronomy, University of California, Berkeley, 501 Campbell Hall 3411, Berkeley, CA, 94720, USA; nr25fran@siena.edu, noahfranz13@gmail.com
[2] Department of Physics and Astronomy, Siena College, 515 Loudon Road, Loudonville, NY 12211, USA
[3] SETI Institute, Mountain View, CA, USA
[4] University of Malta, Institute of Space Sciences and Astronomy, Malta
[5] Department of Physics, University of Wisconsin - La Crosse, 1725 State Street, La Crosse, WI 54601, USA
[6] University of Southern Queensland, Toowoomba, QLD 4350, Australia
[7] International Centre for Radio Astronomy Research, Curtin University, Bentley, WA 6102, Australia
[8] The Breakthrough Initiatives, NASA Research Park, Building 18, Moffett Field, CA, 94035, USA
Received 2021 November 4; revised 2021 December 20; accepted 2021 December 25; published 2022 February 1

Abstract

The Breakthrough Listen (BL) Initiative, as part of its larger mission, is performing the most thorough technosignature search of nearby stars. Additionally, BL is collaborating with scientists working on NASA's Transiting Exoplanet Survey Satellite (TESS) to examine TESS Targets of Interest (TOIs) for technosignatures. Here, we present a 1–11 GHz radio technosignature search of 61 TESS TOIs that were in transit during their BL observation at the Robert C. Byrd Green Bank Telescope. We performed a narrowband Doppler drift search with a minimum S/N threshold of 10 across a drift rate range of ± 4 Hz s^{-1} with a resolution of 3 Hz. We removed radio frequency interference by comparing signals across cadences of target sources. After interference removal, there are no remaining events in our survey, and therefore no technosignature signals of interest detected in this work. This null result implies that at *L*, *S*, *C*, and *X* bands, fewer than 52%, 20%, 16%, and 15%, respectively, of TESS TOIs possess a transmitter with an equivalent isotropic radiated power greater than a few times 10^{14} W.

Unified Astronomy Thesaurus concepts: Technosignatures (2128); Search for extraterrestrial intelligence (2127); Astrobiology (74); Radio astronomy (1338); Exoplanets (498)

1. Introduction

The Search for Extraterrestrial Intelligence (SETI) seeks an answer to the age-old question: Are we alone in the universe? The modern search for technosignatures, or signs of intelligent extraterrestrial life, began in the 1960s (Drake 1961). Due to the limited technology available at the time, this search was restricted to 1420 MHz, which was hypothesized to be a good candidate for a universal communication frequency. However, as technology has developed, technosignature searches have become much more advanced and can cover much wider bandwidths and larger numbers of targets.

The Breakthrough Listen (BL) Initiative, launched in 2015, will search over 1 million targets for technosignatures over its 10 yr lifespan (Worden et al. 2017). BL operates at optical and radio wavelengths, using a wide variety of telescopes including the Robert C. Byrd Green Bank Telescope (GBT) in West Virginia, the Automated Planet Finder in California, and the CSIRO Parkes "Murriyang" 64 m radio telescope in Australia. This work presents a technosignature search of the frequency range 1–11 GHz using the GBT. The BL backend on the GBT is capable of simultaneously delivering billions of frequency channels across several GHz of bandwidth. MacMahon et al. (2018) and Lebofsky et al. (2019) provide information about the instrument, data formats, and post-observation data management.

BL employs a variety of strategies for target prioritization. One is to select targets from catalogs compiled by NASA's Transiting Exoplanet Survey Satellite (TESS). As of 2021 June, TESS has found 4190 new exoplanets, including confirmed exoplanets and candidates, some of which may have suitable conditions for life. Traas et al. (2021) recently performed a technosignature search of 28 TESS targets of interest (TOIs) using the *L*-, *S*-, *C*-, and *X*-band receivers at the GBT. Transiting systems are prioritized because Earth is in the ecliptic for these systems. An ETI may be more likely to send bright signals out in the direction of their ecliptic, either to intentionally signal observers who can see their transits or for purposes such as interplanetary radar (Traas et al. 2021).

We refine the search of Traas et al. (2021) by selecting systems that were observed with the GBT *during* transits of candidate exoplanets, which may further improve the chance of receiving an extraterrestrial signal. An ETI may choose to broadcast signals toward their antistellar point, knowing that observers may be monitoring their system during transit, so there is a higher likelihood of a transmission being received. In addition, by choosing to broadcast at this special temporal "Schelling Point" (Wright et al. 2018; Sheikh et al. 2020; Gajjar et al. 2021), an ETI could enhance signal detectability for a given transmitter power (relative to an omnidirectional transmitter) by increasing their antenna gain and beaming a signal in the opposite direction to their star.

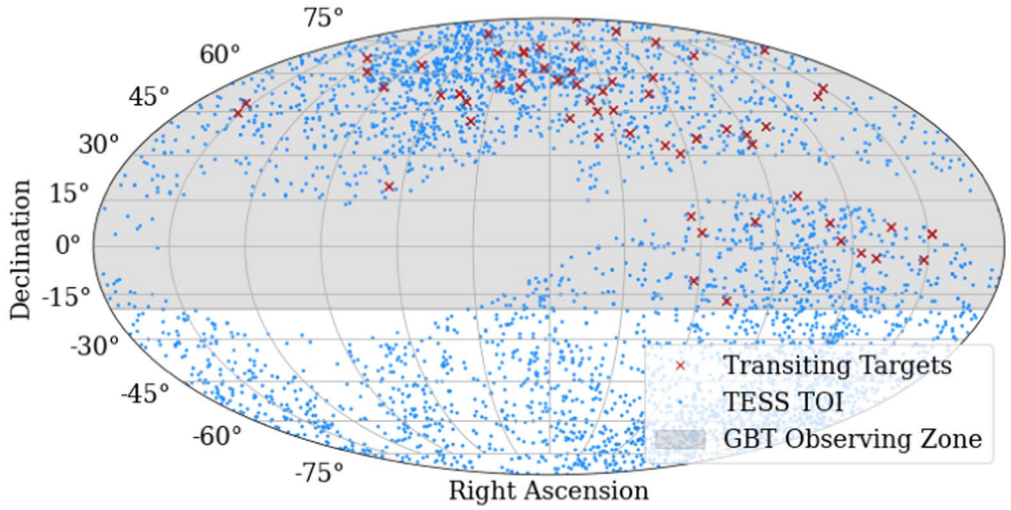

Figure 1. Sky map of all TESS TOIs (blue dots), with transiting TESS targets analyzed in this paper overlaid as red Xs. The gray shaded region is the zone above decl. −20° where BL targets are usually observed with the GBT; BL targets below this decl. are usually observed at the Parkes Observatory.

2. Observations

BL targets at GBT are observed with an "on/off" ABACAD cadence method (Lebofsky et al. 2019). The primary target A is observed, then an "off" target B is observed. This method is then repeated twice more with the same "on" target and two new "off" targets, C and D. Each target in the cadence is observed for 5 minutes such that the "on" target is observed for a total of 15 minutes and each "off" target is observed for 5 minutes. Comparing the "on" and "off" scans allows us to differentiate between radio frequency interference (RFI) signals and a candidate ETI signal, since the latter is expected to be localized on the sky.

2.1. Target Selection

Observations of TOIs by BL at the GBT are scheduled automatically by selection from target lists, and not typically deliberately timed to coincide with transits. By examining ephemerides from ExoFOP-TESS (ExoFOP 2019) for all targets observed by BL at GBT as of 2021 June, we determined[9] that 61 unique targets, across 66 observations, serendipitously transit during their GBT observation. These 61 targets are shown in Figure 1 and the Appendix. TIC 344926234 and TIC 365683032 were observed with two different receivers during two different transits, TIC 376637093 was observed with three different receivers during three different transits, and TIC 286561122 was observed at *C* band twice during a single transit. The notch filter regions (Lebofsky et al. 2019) at *L* (1200–1340 MHz) and *S* (2300–2360 MHz) bands are excluded from our analysis.

A histogram of the fraction of each transit observed is shown in Figure 2. The fraction of transit observed was calculated by dividing the observation time of the entire cadence by the total transit time of the exoplanet candidate,

$$\mathrm{FTO} = \frac{t_{\mathrm{obs,\ transit}}}{(t_{\mathrm{egress}} - t_{\mathrm{ingress}})}, \quad (1)$$

where FTO stands for the Fraction of Transit Observed, $t_{\mathrm{obs,\ transit}}$ is the amount of time in the overlap of the transit time and observation time, and t_{egress} and t_{ingress} are the time of egress and ingress, respectively. Targets that cross the midpoint of their transit, as shown by the hashed bins in Figure 2, are especially interesting: a narrow-beamed transmitter pointing away from the host star, perhaps located at the second Lagrange point, would appear strongest at the midpoint of transit.

Figure 3 shows a histogram of the orbital periods of the TESS TOIs chosen for this project. These periods are all relatively short, so the TOIs are unlikely to be terrestrial planets in the habitable zone. Still, ETI may assume it is easier for us to detect these closer, short-period exoplanets and place a transmitter there.

3. Doppler Search

We perform our analysis on fine-frequency resolution spectrograms from the BL backend at the GBT. As described by Lebofsky et al. (2019) and MacMahon et al. (2018), the BL backend records spectral data in 187.5 MHz frequency chunks, with each chunk sent to a separate compute node. Data recorded before early 2021 were spliced together in frequency, one file per receiver, before archiving. Starting in early 2021, files were instead left in their unspliced form on the compute nodes, which enables easier parallel processing. The 66 cadences analyzed here represent 21 TB of data in total, most of which were analyzed in situ on the GBT BL compute nodes. In one observation in our sample, TIC 365781372 at *X* band, the blc40 compute node failed to record data during a scan, leading to a gap of 187.5 MHz in the spectrum.

Each cadence was analyzed using the BL `turboSETI` pipeline (Enriquez & Price 2019). First, `FindDoppler` identifies narrowband Doppler-drifting signals in the filterbank files. Following from Price et al. (2020) and Traas et al. (2021), we adopt a minimum[10] S/N threshold of 10 across a drift rate range of $\pm 4\ \mathrm{Hz\ s^{-1}}$. To maximize efficiency, we parallelized the processing across all 64 compute nodes available to BL at GBT, greatly reducing run time for large amounts of data.

[9] Code at: https://github.com/noahfranz13/BL-TESSsearch.

[10] `turboSETI`'s dechirping efficiency is lower for high drift rate signals, resulting in a higher effective S/N limit. For more details see Gajjar et al. (2021).

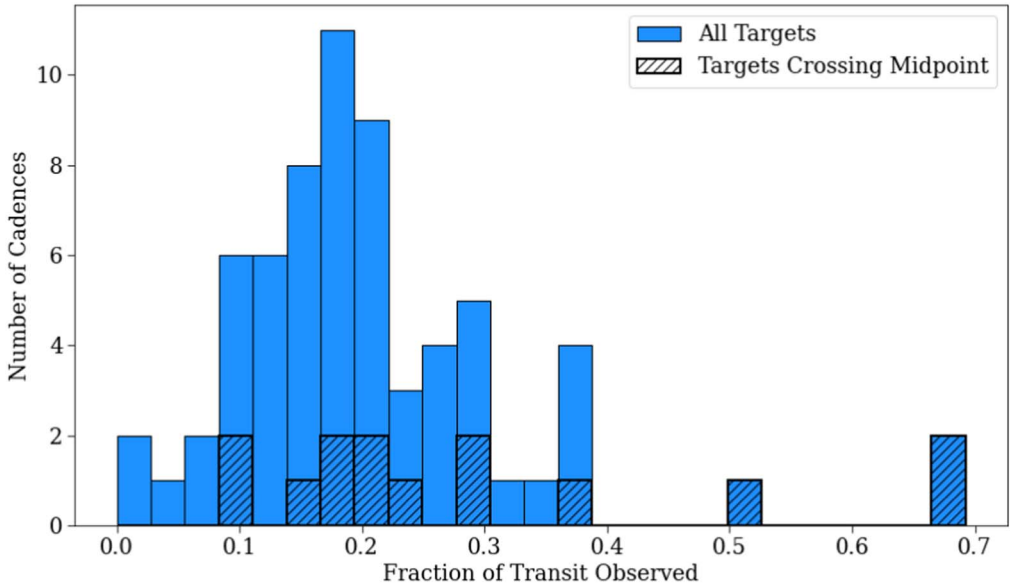

Figure 2. Fraction of the transit observed in the GBT observations. The blue bins represent all 66 cadences, while the hashed bins indicate a target that crosses the midpoint of its transit during the observation.

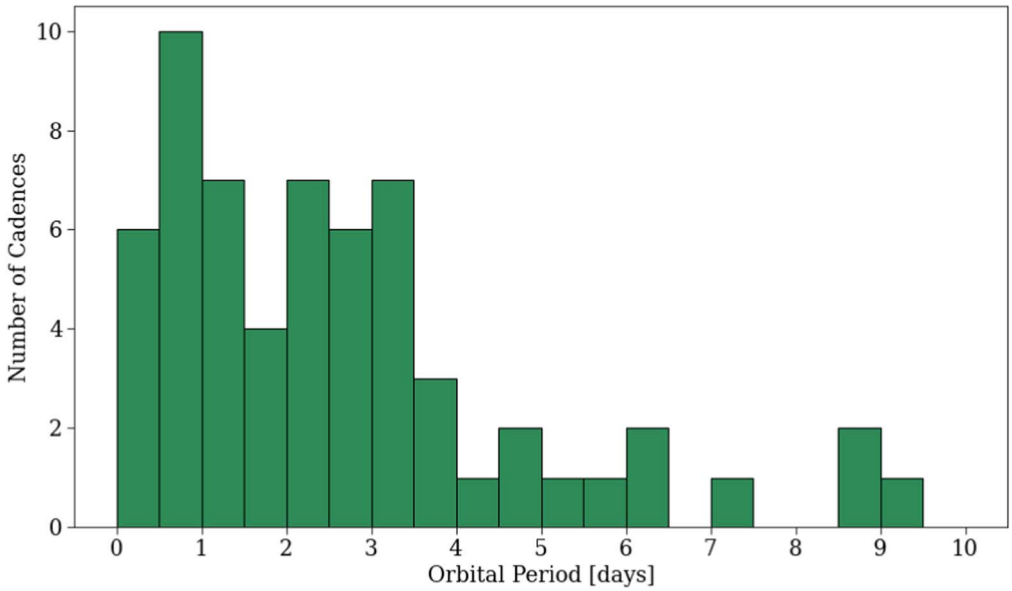

Figure 3. Histogram of the orbital periods of the observed targets.

We use the measured orbital periods for our TOIs, applying the methods presented by Sheikh et al. (2019), to calculate theoretical maximum drift rates for transmitters in the systems in our sample. We neglect any contribution from the rotation rates of the planets (which are unknown, but in many cases may be negligible, since many of our targets have small periods and are most likely tidally locked). We find that only 2.4% of our targets have maximum drift rates that lie within ± 4 Hz s^{-1}, suggesting that a search over a larger drift rate range would be optimal, albeit more computationally expensive. However, it would be simple (and maybe even common) for ETI to correct for their drift rate when transmitting a signal, so received signals would only have small drift rates due to Earth's orbit and rotation (Horowitz & Sagan 1993; Sheikh et al. 2019). Additionally, `turboSETI` will pick out bright signals even if the drift rate is not matched correctly.

The second part of the Doppler search is to run the `find_event` pipeline which removes signals with no drift rate and compares the hits across each cadence, eliminating any signals present in both the "on" and "off" observations. `find_event` returns events, which are any signals that are present in the "on" and not "off" observations. Selecting signals that are only present in the "on" observations removes RFI and isolates signals that are localized on the sky.

Finally, the `plot_event` pipeline produces cadence plots for visual inspection, which allows us to manually eliminate any RFI remaining after the `find_event` pipeline. For more information see Enriquez et al. (2017) and Enriquez & Price (2019).

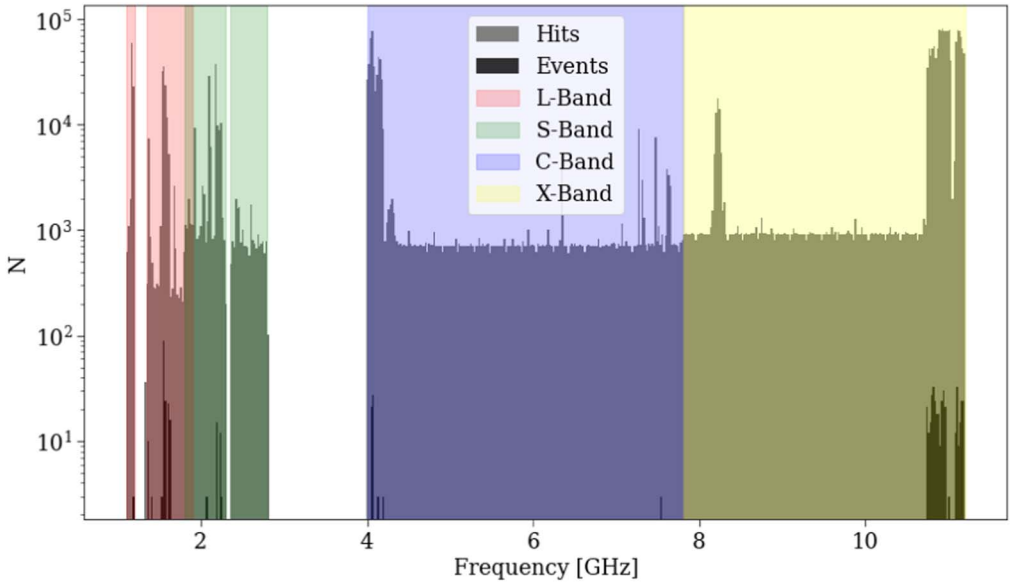

Figure 4. Number of hits (gray) and events (black) vs. frequency. The frequency range (band) for each GBT receiver is represented by the colored regions; the (unshaded) notch filter regions (Lebofsky et al. 2019) at *L* and *S* bands are excluded from our analysis. Values for each band, with the number of cadences, are shown in Table 1. Note that there are a different number of cadences at each band so the number of hits and events plotted here should not be directly compared across bands.

Table 1
Survey Parameters

Receiver	Frequency (GHz)	Cadences	Hits	Events	CWTFM[a]	10σEIRP$_{min}$ (TW)[b]	Transmitter Limit (%)[c]
L	1.10–1.90	5	213097	172	3793	167	52
S	1.80–2.80	17	160057	33	2828	393	20
C	4.00–7.80	21	578264	57	3060	788	16
X	7.80–11.20	23	1503241	372	3686	719	15
Total	1.10-11.20	66	2442347	634	…	…	…

Notes.
[a] Continuous Waveform Transmitter Figure of Merit (CWTFM) is a figure of merit that describes the likelihood to find a signal above the EIRP$_{min}$ for that receiver.
[b] Minimum Equivalent Isotropic Radiated Power (EIRP$_{min}$) is a measure of the minimum necessary omnidirectional power of a transmitter at each receiver to be detected.
[c] The transmitter limit is the maximum percentage of exoplanet candidates in each frequency range that possess a transmitter.

4. Results

4.1. Technosignature Search

For the rest of this discussion, we refer to a "hit" as any signal present in a single observation and an "event" as a collection of related hits that successfully passed through the `find_event` pipeline. We find 2,442,347 hits and 634 events which were distributed across the receiver bands as shown in Figure 4 and Table 1. We show examples of events in Figure 5. After visually inspecting all 634 events, we find that all of them are consistent with human-generated RFI. Most commonly, these signals appear to be present—but not detectable by `turboSETI` above the S/N threshold—throughout the entire cadence, indicating a source of interference that is likely local to the telescope.

Figures 5(a) and 5(b) illustrate signals that seem to appear mostly in the "on" observations in a given cadence. However, both cadences also have some similar signals in the "off" observations and can therefore be ruled out as signals of interest. These signals are broader in frequency than the narrowband drifting tones `turboSETI` is designed to search for. Nevertheless, they were bright enough to rise above `turboSETI`'s S/N threshold and register as hits. Although an ETI could transmit signals with a range of bandwidths, the broader signals in this study were clearly due to RFI. Furthermore, the signal in Figure 5(a) is in a frequency range commonly used for aeronautical radar (as are many of the top-ranked events presented by Enriquez et al. 2017). Likewise, Figure 5(b), given its frequency, is RFI that is likely related to the Iridium satellite constellation.

Figure 5(c) shows a waterfall plot of TIC 241076290, a candidate exoplanet with a tight orbit around its host star, with a period of 0.258 days. This is the only target in our analysis whose transit is shorter than the 30 minute observation. In this case we observe only the end of the transit. In the future, by scheduling specifically timed observations for systems with short transits, we could look for signals that appear only during transit. As of 2021 June, in the ExoFOP-TESS catalog there are 31 TOIs with transits shorter than 30 minutes, which corresponds to 0.74% of TOIs. These TOIs would be interesting targets for follow-up observations.

Figure 5(d) appears to have a nonlinear Doppler shift, suggesting it is accelerating with respect to the telescope, as might be expected for a satellite in Earth orbit, and its

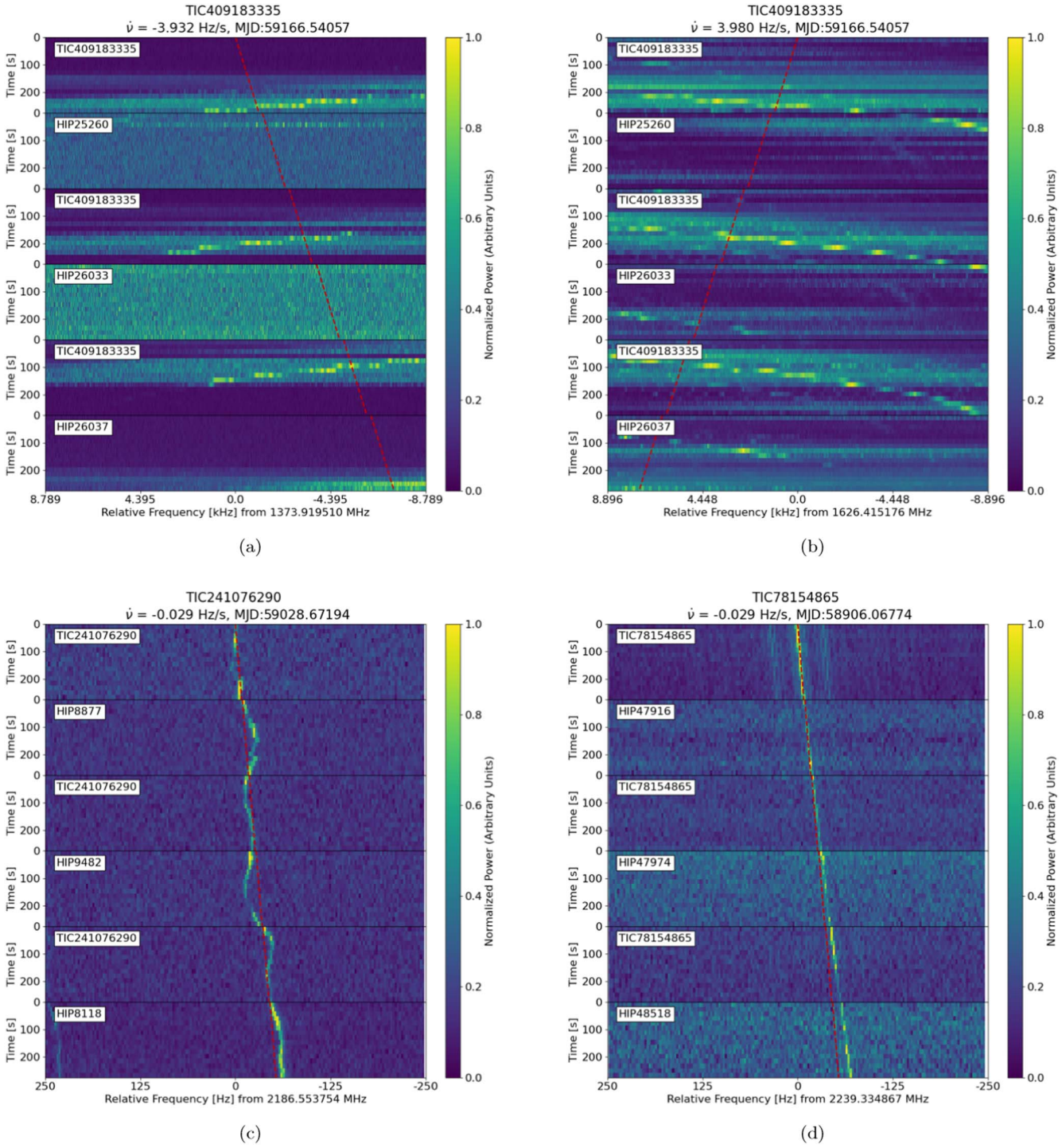

Figure 5. Dynamic spectra (waterfall plots) of four representative events from the 634 event sample. Each plot is a vertical stack of the 6 scans making up an ABACAD cadence. The vertical axis shows the time since the start of each scan in the cadence, and the horizontal axis shows the frequency offset from the event's starting frequency.

frequency corresponds to a known satellite downlink frequency. However, due to the relative motion of satellites (even geosynchronous satellites) with respect to sidereal targets, they usually appear in only one or two scans. Instead, Figure 5(d) has a signal present throughout the entire cadence. Its presence in the "off" scans rules it out as an ETI candidate; it may be a pernicious example of a slow-moving satellite (possibly visible through a telescope sidelobe) that was moving in the same general direction as the telescope over the course of the 30 minutes observation.

4.2. Hit and Event Distribution

The hit and event frequency distributions are shown in Figure 4. Histograms of the S/N and drift rate distributions are shown in Figure 6. There are significantly more hits and events at low drift rates, likely produced by RFI local to the telescope.

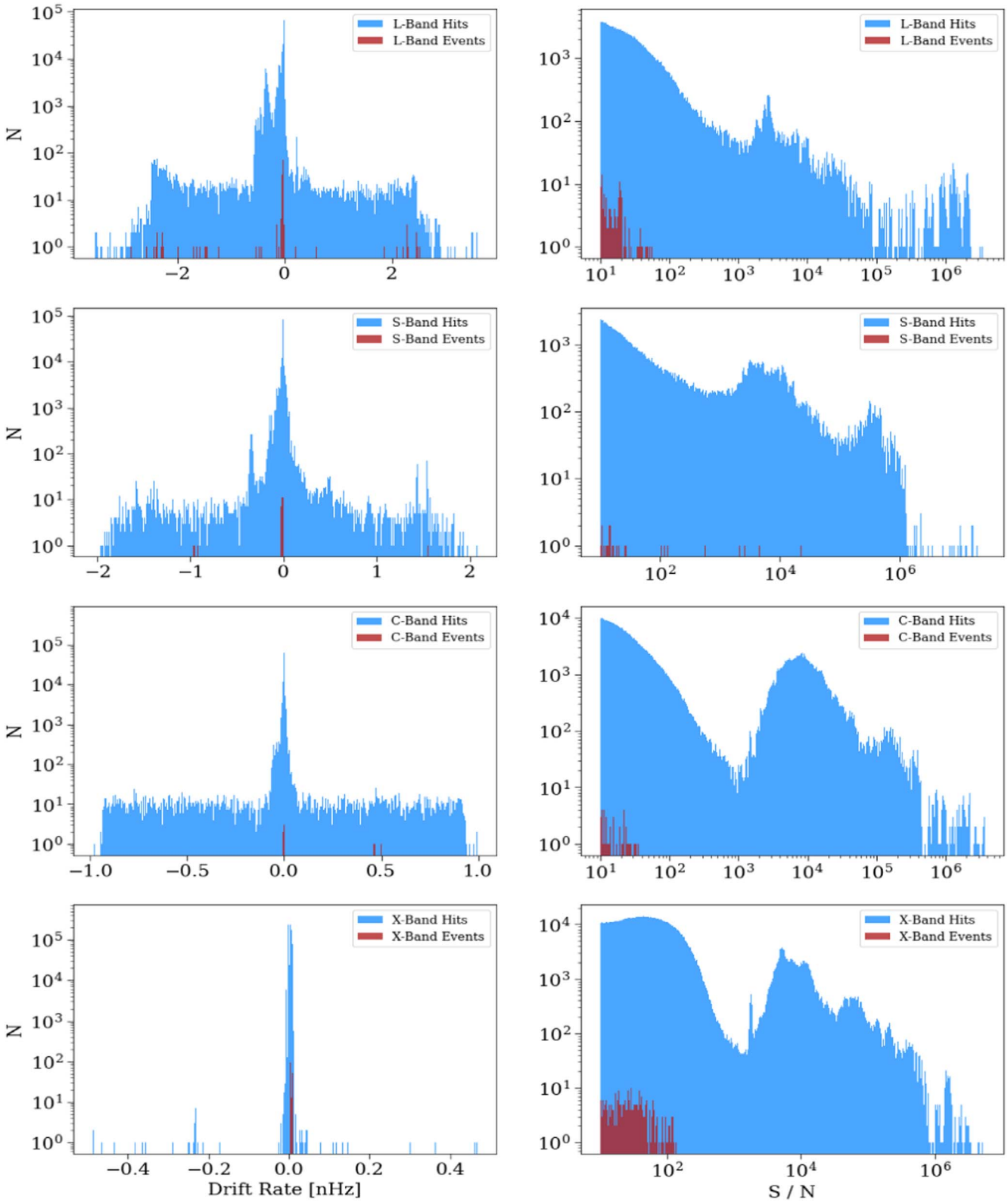

Figure 6. Left: histograms of hits (blue) and events (red) as a function of drift rate split up by receiver. The reported drift rate is normalized by the center frequency of the hit or event, to produce a value in units of nHz (e.g., 1 nHz = 1 Hz s^{-1} at 1 GHz). Right: histograms of hits (blue) and events (red) as a function of S/N split up by GBT receiver. Note that not all receivers observed the same number of targets.

4.3. Figures of Merit

To further evaluate our ability to detect ETI signals in this work, we can compare our figures of merit to those from past SETI studies. One such figure of merit is the Drake Figure of Merit (DFM; Drake et al. 1984),

$$\mathrm{DFM} = \frac{n\,\Delta f\,\Omega}{F_{\mathrm{min}}^{3/2}}, \tag{2}$$

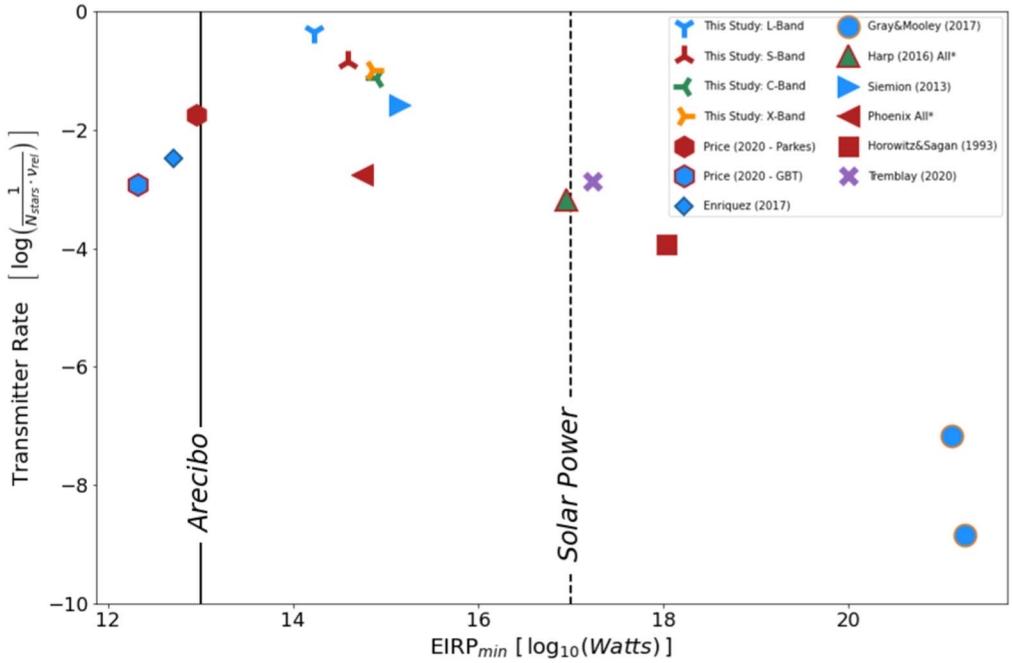

Figure 7. Transmitter Rate vs. $\mathrm{EIRP_{min}}$ for this study (represented by the four Y-shaped points) compared to past studies (none of which specifically targeted systems during transits). The two vertical lines represent the EIRP of the Arecibo *S*-band radar, and the solar power incident on Earth.

Table 2
Drake Figure of Merit

Study	DFM [GHz $\mathrm{m^3}$ $\mathrm{W^{3/2}}$]
This Study	2.1×10^{32}
Margot et al. (2021)	1.11×10^{32}
Gajjar et al. (2021)	4×10^{28}

where n is the number of observations at a receiver, Δf is the total frequency range observed, Ω is the FWHM of the receiver, and F_{min} is the minimum detectable flux. While DFM has some limitations, as discussed by Enriquez et al. (2017) and Margot et al. (2021), it is still a useful statistic, especially for surveys across multiple receivers, such as this one, because it incorporates both the bandwidth surveyed and the minimum detectable power. Table 2 shows the DFM for this study in comparison to other recent searches; larger DFMs indicate more comprehensive searches.

A second useful figure of merit is the Continuous Waveform Transmitter Figure of Merit (CWTFM; Enriquez et al. 2017). This describes the likelihood of finding an ETI signal above a specific minimum Equivalent Isotropic Radiated Power ($\mathrm{EIRP_{min}}$),

$$\mathrm{CWTFM} = \zeta_{\mathrm{AO}} \frac{\mathrm{EIRP_{min}}}{N_{\mathrm{stars}}\, \nu_{\mathrm{rel}}}, \tag{3}$$

where N_{stars} is the number of pointings in a survey at a receiver times the number of stars per pointing (assumed to be 1), ν_{rel} is the total bandwidth for a receiver normalized by the central frequency of the receiver, and ζ_{AO} is a normalization constant such that CWTFM is 1 for an EIRP equal to that of Arecibo. $\mathrm{EIRP_{min}}$ is a measure of the necessary power of a hypothetical omnidirectional antenna, in the most distant star system in our sample, to be detected by each GBT receiver. We plot the Transmitter Rate (CWTFM divided by $\mathrm{EIRP_{min}}$) versus $\mathrm{EIRP_{min}}$ for our study in comparison to past searches in Figure 7. Technosignature searches represent compromises between sensitivity (higher sensitivity toward the left-hand side of the figure) and sky and bandwidth coverage (more stars, and/or wider fractional bandwidth coverage, toward the bottom of the figure). Our study occupies a similar region of parameter space to previous studies, but is the first to achieve wide frequency coverage for a significant number of stars observed during the transit of candidate exoplanets.

4.4. Transmitter Limit

Given our lack of detection of any signal of interest, we can calculate the transmitter limit, or maximum percentage of TESS TOIs at each band that possess a detectable transmitter based on our search parameters. Price et al. (2020), Traas et al. (2021), and other authors calculate this limit using a one-sided 95% Poisson confidence interval with a 50% probability of actually observing a signal if the transmitter is present (Gehrels 1986). Given the small number of cadences observed at the *L* band, a binomial confidence interval is a better estimate for the transmitter limit in our case. We list the relevant limits (95% one-sided binomial interval, with a 50% probability of detecting a signal if present) in Table 1. Work is ongoing to determine more accurate detection thresholds by performing signal injection and recovery in BL data.

The TOIs observed in this work all have short periods, as shown in Figure 3. These targets are very close to their host stars, receiving many hundreds of times more stellar insolation than terrestrial planets in the habitable zone. Additionally, some of our targets are exoplanet candidates rather than confirmed exoplanets. Some caution is therefore warranted in extrapolating the transmitter limits from the TESS TOIs observed in this work to the entire population of exoplanets.

5. Conclusions

We performed a technosignature search of 61 TESS TOIs, over 66 observations, that are in transit during their BL observation at the GBT. This could be a favored time to search for technosignatures from ETI because Earth is in the ecliptic of these exoplanet candidates as they transit. ETIs may determine such transits are good Schelling Points, and time their transmissions accordingly.

After searching the 66 cadences for technosignatures, we did not find any potential technosignature signals of interest. Using this null result, we constrain the existence of extraterrestrial transmitters brighter than a few hundred TW to less than 52%, 20%, 16%, and 15% (for *L*, *S*, *C*, and *X* bands, respectively) of TESS TOIs that are observed during transit.

6. Future Studies

There are numerous ways to extend the work presented in the previous sections. First, we could analyze targets that serendipitously enter or exit their secondary transit during their observation. This way, we could search for signals that appear or disappear as the exoplanet candidates pass behind its host star.

Second, we could search for signals that appear or disappear at the same time as targets enter or exit their transit during a BL observation. This would require observations that cover the entire transit, including a substantial portion of data taken outside of the ingress and egress of the transit. Since ETI may assume that Earth is observing the exoplanet during its transit, they may transmit a beacon to Earth only during the transit.

Third, we could search for signals that appear close to the midpoint of the transit as viewed from Earth. In this scenario, ETI may direct a narrow, beamed signal toward their antistellar point, which might appear as a signal that changes in intensity with a Gaussian shape, as Earth is swept by the transmitter beam. Such a signal could come from a transmitter present on the antistellar point of a tidally-locked planet or, as previously mentioned, a transmitter placed at an exoplanet's second Lagrange point.

Fourth, rather than rely on serendipitous scheduling of BL observations of TESS TOIs, observations could be scheduled during exoplanet candidate transits. This could enable larger, more thorough studies of exoplanet candidate transits as a Schelling Point, and as a geometrically favorable region for technosignature searches.

The Breakthrough Prize Foundation funds the Breakthrough Initiatives which manages Breakthrough Listen. The Green Bank Observatory facility is supported by the National Science Foundation, and is operated by Associated Universities, Inc. under a cooperative agreement. We thank the staff at Green Bank Observatory for their support with operations. N.F. was funded as a participant in the Berkeley SETI Research Center Research Experience for Undergraduates Site, supported by the National Science Foundation under grant No. 1950897. This research has made use of the Exoplanet Follow-up Observation Program website, which is operated by the California Institute of Technology, under contract with the National Aeronautics and Space Administration under the Exoplanet Exploration Program.

N.F. thanks all of the 2021 Berkeley SETI interns for their support and encouragement. In addition, we thank Richard Elkins for his support with running `turboSETI` and Daniel Estévez for his insight in identifying the signal in Figure 5(d). We thank the anonymous referee for their comments on the manuscript.

Appendix
Target List

In Table A1 we provide the list of targets observed.

Table A1
Our Sample of TESS TOIs that Transited During their Observation at the GBT

Target Name	TOI	R.A. (hr)	Decl. (°)	Distance (pc)	Orbital Period (days)	Observation Start Time (UTC)	Band
TIC438490744	529.01	6.683726312	16.58970997	63.0507	1.665878	5/31/2021 21:36	*C*
TIC147950620	1194.01	11.18809073	69.96478246	149.667	2.310602	6/14/2020 20:37	*C*
TIC458478250	1165.01	15.47643744	66.35871037	126.261	2.255296	11/24/2019 23:54	*S*
TIC344926234	634.01	10.10383058	3.946493286	92.8368	0.49359	11/24/2019 14:43	S, *C*
TIC78154865	638.01	9.857820581	−4.123319468	96.6355	0.493826	2/27/2020 1:37	*S*
TIC365781372	627.01	5.461566558	7.918525328	629.834	1.13889	11/30/2019 5:03	*X*
TIC270468559	571.01	9.022952699	6.097088972	405.238	4.641843	9/11/2020 19:08	*C*
TIC121338379	498.01	8.606046796	−3.860202132	188.364	0.275043	1/19/2020 8:34	*S*
TIC375542276	1163.01	19.60611228	19.63922729	148.342	3.07765	12/15/2019 1:12	*L*
TIC468880077	438.01	3.766972039	9.9903089	72.4646	5.8076	1/27/2021 23:58	*C*
TIC459942762	430.01	4.018554669	4.540889327	66.5727	0.58644	12/21/2019 6:56	*X*
TIC280437559	969.01	7.675771778	2.098612197	77.2554	1.823737	1/11/2020 9:20	*X*
TIC425206121	508.01	7.433963292	7.615772707	300.276	4.611733	1/19/2020 3:44	*S*
TIC178367144	966.01	8.226143814	−1.982782058	253.985	3.409244	1/19/2020 8:02	*S*
TIC138168780	1651.01	6.319529079	73.82755828	235.479	3.764988	3/29/2021 18:57	*L*
TIC73104318	1674.01	4.114769716	58.46544652	201.645	7.45494	2/10/2020 4:40	*X*
TIC422756130	1695.01	1.461444537	72.29660211	45.1309	3.134319	5/25/2020 18:35	*S*
TIC285674856	1570.01	3.546414139	51.88450172	294.123	1.74626	2/17/2020 20:06	*X*
TIC241076290	1560.01	1.935519308	52.58547107	560.222	0.25792	6/28/2020 16:07	*S*
TIC348673213	1639.01	2.387149453	56.57002561	153.986	0.901465	4/19/2020 16:04	*C*
TIC292321872	1572.01	2.126808592	45.50016306	505.331	8.66698	11/13/2020 9:44	*L*
TIC294471966	1446.01	20.1334245	51.36180671	133.863	6.31719	6/30/2020 0:34	*C*

Table A1
(Continued)

Target Name	TOI	R.A. (hr)	Decl. (°)	Distance (pc)	Orbital Period (days)	Observation Start Time (UTC)	Band
TIC409183335	1667.01	5.453849363	38.59745582	225.941	3.32125	11/13/2020 12:58	*L*
TIC286561122[a]	1658.01	4.391744889	35.49511432	506.864	0.67994	3/23/2020 0:16	*C*
TIC311035838	1419.01	13.73959477	48.02856107	134.554	2.899733	6/20/2020 5:37	*S*
TIC327579226	1532.01	0.315744444	57.20064898	259.563	8.90592	11/10/2020 4:26	*X*
TIC365683032	1354.01	20.81199235	51.91068918	245.776	1.42904	4/18/2020 8:56	*S*, *X*
TIC241040309	1559.01	1.381155015	48.95536157	685.251	3.46479	7/18/2020 13:06	*X*
TIC312862941	1638.01	1.021431709	55.69799904	126.283	0.915094	4/20/2020 0:22	*C*
TIC137881699	1781.01	10.03817034	53.95082988	935.456	2.972133	9/11/2020 23:33	*C*
TIC149833117	1717.01	6.975231953	67.67733006	188.086	4.052173	6/5/2020 4:12	*S*
TIC368536386	1666.01	5.961338651	36.76580927	428.948	1.69433	9/14/2020 7:13	*C*
TIC376682699	1511.01	22.69014554	69.07445015	544.233	1.10264	11/8/2020 15:36	*X*
TIC376637093	1516.01	22.67230188	69.50372602	247.054	2.05603	5/19/2020 22:39	*S*, *C*, *X*
TIC327011842	1576.01	1.564455335	45.01032893	493.702	0.78424	7/18/2020 11:58	*X*
TIC44631965	1461.01	1.482420079	35.86484113	359.959	3.568678	5/29/2020 19:06	*C*
TIC142090065	1715.01	5.271560572	79.73772521	182.907	2.826937	9/4/2020 7:39	*X*
TIC198212955	1242.01	16.57021523	60.19589615	110.015	0.381481	7/29/2020 8:39	*C*
TIC138017750	1608.01	3.386736393	33.07814949	100.635	2.472722	10/26/2020 0:59	*S*
TIC26433869	1607.01	3.7876164	30.14950686	329.591	1.03578	7/3/2020 18:25	*X*
TIC353367071	1663.01	5.995649857	33.50698402	402.261	2.37532	9/14/2020 8:18	*C*
TIC272625214	1613.01	23.75456899	62.14267079	304.76	5.24666	7/27/2020 16:11	*C*
TIC129979528	1599.01	2.447511416	37.55044553	121.944	1.219868	9/17/2020 7:05	*X*
TIC341815767	1819.01	17.83467483	54.63614716	160.295	3.09374	12/21/2020 19:24	*X*
TIC457138169	1770.01	9.424525742	50.9088635	163.438	1.09254	8/14/2020 13:08	*C*
TIC371673488	1497.01	22.88221213	59.85095835	405.174	0.8158	12/20/2020 1:44	*X*
TIC15863518	1713.01	6.701367042	39.84291832	138.371	0.557201	12/13/2020 0:47	*X*
TIC389182138	1391.01	22.90899711	54.16180798	115.746	2.72687	10/10/2020 6:51	*C*
TIC235905185	1829.01	19.39182508	78.75421665	479.529	6.289555	12/1/2020 4:15	*X*
TIC191284318	1458.01	0.63819763	42.46306636	226.637	2.77598	11/10/2020 7:20	*X*
TIC358631536	1343.01	21.17169156	48.4642791	400.034	3.40304	12/24/2020 18:22	*S*
TIC274942910	1325.01	21.52843349	41.79747049	52.4946	1.07922	12/24/2020 22:09	*S*
TIC233720539	1815.01	18.42528104	63.48810973	617.233	2.55532	1/14/2021 1:44	*X*
TIC38686737	432.01	3.857704881	−10.6140933	746.646	2.24704	1/14/2021 5:19	*X*
TIC117979455	422.01	4.786847839	−17.25336165	124.504	0.63322	1/17/2021 5:29	*S*
TIC328167090	1384.01	22.11089078	55.68625098	235.218	0.71255	4/4/2021 13:04	*L*
TIC154741689	2170.01	10.95424616	89.08691789	206.368	9.27688	3/17/2021 6:56	*C*
TIC427730490	2040.01	23.48497742	71.50646786	144.717	3.86085	3/22/2021 20:38	*X*
TIC321688498	2290.01	21.43996743	68.64052458	58.0924	0.38623	3/22/2021 22:53	*X*
TIC393911494	2106.01	13.81189142	44.9117615	121.167	0.633259	3/28/2021 11:38	*S*
TIC285542903	2060.01	0.884664039	60.61811644	914.062	2.26584	4/19/2021 17:49	*C*

Note.
[a] Note that this target was observed twice at *C* band and both cadences overlap transits for this TOI.

ORCID iDs

Noah Franz https://orcid.org/0000-0003-4537-3575
Steve Croft https://orcid.org/0000-0003-4823-129X
Andrew P. V. Siemion https://orcid.org/0000-0003-2828-7720
Raffy Traas https://orcid.org/0000-0002-3364-7009
Bryan Brzycki https://orcid.org/0000-0002-7461-107X
Vishal Gajjar https://orcid.org/0000-0002-8604-106X
Howard Isaacson https://orcid.org/0000-0002-0531-1073
Matthew Lebofsky https://orcid.org/0000-0002-7042-7566
Danny C. Price https://orcid.org/0000-0003-2783-1608
Sofia Z. Sheikh https://orcid.org/0000-0001-7057-4999

References

Backus, P. R. & Project Phoenix Team 2004, BAAS, 36, 805
Drake, F. 1961, PhT, 14, 40
Drake, F., Wolfe, J. H., & Seeger, C. L. 1984, SETI Science Working Group Report, Technical Report 2244, Scientific and Technical Information Office, https://ntrs.nasa.gov/citations/19840014110
Enriquez, E., & Price, D. 2019, turboSETI: Python-based SETI search algorithm, Astrophysics Source Code Library, ascl:1906.006
Enriquez, J. E., Siemion, A., Foster, G., et al. 2017, ApJ, 849, 104
ExoFOP 2019, Exoplanet Follow-up Observing Program-TESS, IPAC, doi:10.26134/ExoFOP3
Gajjar, V., Perez, K. I., Siemion, A. P. V., et al. 2021, AJ, 162, 33
Gehrels, N. 1986, ApJ, 303, 336
Gray, R. H., & Mooley, K. 2017, AJ, 153, 110
Harp, G. R., Richards, J., Tarter, J. C., et al. 2016, AJ, 152, 181

Horowitz, P., & Sagan, C. 1993, ApJ, 415, 218
Lebofsky, M., Croft, S., Siemion, A. P. V., et al. 2019, PASP, 131, 124505
MacMahon, D. H. E., Price, D. C., Lebofsky, M., et al. 2018, PASP, 130, 044502
Margot, J.-L., Pinchuk, P., Geil, R., et al. 2021, AJ, 161, 55
Price, D. C., Enriquez, J. E., Brzycki, B., et al. 2020, AJ, 159, 86
Sheikh, S. Z., Siemion, A., Enriquez, J. E., et al. 2020, AJ, 160, 29
Sheikh, S. Z., Wright, J. T., Siemion, A., & Enriquez, J. E. 2019, ApJ, 884, 14
Siemion, A. P. V., Demorest, P., Korpela, E., et al. 2013, ApJ, 767, 94
Traas, R., Croft, S., Gajjar, V., et al. 2021, AJ, 161, 286
Tremblay, C. D., & Tingay, S. J. 2020, PASA, 37, e035
Worden, S. P., Drew, J., Siemion, A., et al. 2017, AcAau, 139, 98
Wright, J. T., Sheikh, S., Almár, I., et al. 2018, arXiv:1809.06857